Korean Journal of Remote Sensing, Vol.20, No.3, 2004, pp.215~225

Unsupervised Image Classification using Region-growing Segmentation based on CN-chain

Sang-Hoon Lee

Department of Industrial Engineering, Kyungwon University

Abstract : A multistage hierarchical clustering technique, which is an unsupervised technique, was suggested in this paper for classifying large remotely-sensed imagery. The multistage algorithm consists of two stages. The "local" segmentor of the first stage performs region-growing segmentation by employing the hierarchical clustering procedure of CN-chain with the restriction that pixels in a cluster must be spatially contiguous. The "global" segmentor of the second stage, which has not spatial constraints for merging, clusters the segments resulting from the previous stage, using the conventional agglomerative approach. Using simulation data, the proposed method was compared with another hierarchical clustering technique based on "mutual closest neighbor." The experimental results show that the new approach proposed in this study considerably increases in computational efficiency for larger images with a low number of bands. The technique was then applied to classify the land-cover types using the remotely-sensed data acquired from the Korean peninsula.

Key Words : Classification, Hierarchical Clusteringusing, Mutual Closest Neighbor, CN-chain, Region-growing, Segmentation, Remote Sensing.

1. Introduction

Most approaches to the image classification require *a priori* class-dependent knowledge of parameterized models for the data. In many instances, however, the parameter values of the models are not known *a priori*, and the process of gathering training samples to estimate parameters is often infeasible or very expensive. In addition, the classification results much depend on the number of classes selected in the specific analyzed area, but it is very complicate to determine the class number, as known as "cluster validation," particularly for remotely sensed data. Therefore, it is necessary that classification procedures perform the unsupervised learning of the parameters including the number of classes and the image classification simultaneously. For the unsupervised analysis, agglomerative hierarchical clustering technique (Anderberg, 1973) is one of the most appropriate approaches.

Image segmentation/classification methods typically assume that a hierarchy exists in the scene information. Under the constraint of hierarchical structure, it is then possible to determine natural image segments by combining hierarchical clustering with region-growing/merging. The general procedure of region-growing/merging involves comparison of one pixel or

Received 10 May 2004; Accepted 11 June 2004.

region with its spatial neighbor(s), and assigning it to the same class based on a criterion of homogeneity or a statistical similarity measure. Adams and Bischof (1994) presented the "seeded region growing" (SRG) technique, which is controlled by a number of initial seeds without tuning homogeneity parameters as in conventional region-growing. Chang and Li (1994) proposed another region-growing framework that similarly requires no parameter tuning or prior knowledge about the image, but where the region-growing process is guided by regional feature analysis. Hojjatoleslami and Kittler (1998) developed an approach with a unique feature that in each step at most one candidate pixel exhibits the required properties to join the region. Hybrid techniques combining edge detection and region-growing/merging have also been proposed as a means of achieving improved segmentation of images. For example, Pavlidis and Liow (1990) developed a method to merge segments obtained from a region-growing approach by eliminating or modifying the edges between regions based on a homogeneity criterion. Fan *et al.* (2001) also proposed a hybrid technique that integrates the results of edge extraction and those of SRG, where the centroids between the regions defined by the edges are used as the initial seeds for the SRG procedure. Other schemes for hybrid segmentation were introduced in (Haris *et al.*, 1998; Zhu and Yullie, 1996). Haris *et al.* used watershed segmentation and fast region-merging, and Zhu and Yuille presented an approach called "region competition" which combines aspects of snakes/ balloons and region-growing.

Due to advances in sensor technology, it is now possible to acquire high-resolution data over large geographical area. The high-resolution imagery possesses much detailed spatial information, but one of challenging problems in processing this large dimensional data is the computational complexity resulting from processing the vast amount of data volume. Especially, the unsupervised classification that makes use of hierarchical clustering may require enormous processing time for large images. Lee (2001) used a multistage classification approach based on regional growing, which is computationally efficient for the unsupervised classification. The multistage algorithm includes two stages of segmentation. The first stage performs region-growing segmentation that confines merging to spatially adjacent clusters and then generates an image partition such that no union of any neighboring segments is uniform The "local" segmentor employs a hierarchical clustering procedure that merge the best "mutual closest neighbor (MCN)" pair satisfying a given clustering criterion. In the second stage, the image partition resulting from the regional segmentation is classified into a small number of distinct states by a sequential merging operation. The "global" segmentor uses the conventional agglomerative hierarchical clustering scheme that merges step-by-step small two regions into a large one. To alleviate the memory problem and improve the computational performance of the algorithm, this approach uses a multi-window strategy of boundary blocking operation by constructing a pyramid-like hierarchy system.

In Lee (2001), the clustering procedure in the regional segmentation performs the search for the best pair to be merged among all the MCN pairs and update the set of MCN pairs at every iteration. It may result in computational inefficiency for the segmentation. This study suggested another approach to find the pairs to be merged in the clustering procedure of the regional segmentation. The new method links two adjacent regions that are a MCN pair, using "closest neighbor chain (CN-chain)." It does not require the search of the best pair and the update of the set of MCN pairs. This paper is organized as follows. Section 2 contains a description of the CN-chain spatial clustering for image segmentation. The hierarchical clustering for unsupervised classification is presented in Section 3.

Experimental results with both simulated data and remotely-sensed data are reported and discussed in Section 4. Finally, conclusions are stated in Section 5.

2. CN-chain Spatial Clustering

The computational efficiency of hierarchical clustering segmentation is mainly dependent on how to find the best pair to be merged. Let $I_n = \{1, 2, \cdots, n\}$ be an index set of pixels of a sample image, $J_M = \{1, 2, \cdots, M\}$ be an index set of regions associated with $G_J = \{G_j \subseteq I_n \mid j \in J_M\}$ that is a partition of I_n, $R_J = \{R_j \subseteq I_n \mid j \in J_M\}$ be a region neighborhood system such that R_j is the index set of neighborhood regions of region j. The closest neighbor of region j is defined as

$$CN(j) = \arg\min_{k \in R_j} d(j, k) \quad (1)$$

where $d(j, k)$ is the dissimilarity measure between regions j and k, and R_j is the index set of regions considered to be merged with region j. The pair of regions is then defined as MCN iff $k = CN(j)$ and $j = CN(k)$. If a cutting rule that

$$CR(j, k) < CR_{max} \quad (2)$$

is given as a merging condition of two regions, for any arbitrary region r_0 satisfying $CR(r_0, r_1) < CR_{max}$, a CN-chain is established as the sequence of regions

$$r_0, r_1 = CN(r_0), r_2 = CN(r_1), \cdots, r_{h-1} = MCN(r_h) \quad (3)$$

such that the last two region constitutes an MCN pair, i.e.

$$r_{h-1} = CN(r_h) \text{ and } r_h = CN(r_{h-1}).$$

The sequence of (3) also satisfies

$$CR(r_{k-1}, r_k) < CR_{max} \text{ for } k = 1, 2, \cdots, h.$$

The CN-chain algorithm is outlined in the following:

1. Initialize that every pixel is defined as a region, i.e., $J_M \leftarrow I_n$.
2. Construct a CN-chain by starting the region r_0 with the lowest index among J_M satisfying
   $CR(r_0, CN(r_0)) < CR_{max}$.
   If there exists no available region, STOP.
3. Merge the last MCN pair, r_{h-1} and r_h by indexing the new region with the lower one of both region indices and update the partition by eliminating the region with the higher index, i.e.
   $r_{new} \leftarrow \min\{r_h, MCN(r_h)\}$
   $J_M \leftarrow J_M \backslash q$ where $q = \max\{r_h, MCN(r_h)\}$,
   and update the regional parameters of the new region r_{new}.
4. For $h = 1$,
   if $CR(r_0, CN(r_0)) < CR_{max}$, reconstruct the CN-chain from the starting region r_0.
   else GOTO Step 2.
   For $h > 1$,
   if $CR(r_{h-2}, CN(r_{h-2})) < CR_{max}$, reconstruct the CN-chain from the starting region r_{h-2}.
   else GOTO Step 2.
5. GOTO Step 3.

One common objective in image segmentation involves minimizing the over-all intra-cluster sample variance. This results in the maximum likelihood solution for the case of unknown parameters in a Gaussian image field. Other statistical measures can also be employed to obtain well-posed solutions, but at a higher computational cost (Lee and Crawford, 2005). The advantages of intra-cluster sample variance are both simplicity and its ability to represent a basic important characteristic of clusters. In the local segmentation of spatial region-growing, this study assumes a simple variance structure with no correlation between bands for the image data processes. Under this assumption, the dissimilarity measure based on the intra-cluster sample variance is defined:

$$d(r, s) = \frac{n_r n_s \sum_{k=1}^{b} (\hat{\mu}_{rk} - \hat{\mu}_{sk})^2}{n_r + n_s} \quad (5)$$

where b is the number of bands, n_j and $\hat{\mu}_{jk}$ are the number of pixels and the kth band's average of G_j respectively.

It is difficult to define an appropriate measure of homogeneity to establish rules for cutting the hierarchical tree. The model fitting approaches using information criteria which measure the trade-off between the likelihood and the penalty for increasing the model's order have been applied for cluster validation in image analysis (Won and Derin, 1992). One of these approaches involves selecting the optimal state that maximizes Schwarz's information criterion (Schwarz, 1978):

$$\mathrm{SIC} = -2\log L(h) + K(h)\log n \tag{6}$$

where h is the number of distinct states, $L(h)$ and $K(h)$ are the maximum value of the likelihood function and the number of independent parameters estimated when using h states respectively. The SIC statistic was derived assuming a nonzero prior based on an asymptotic approximation to Bayes' loss. Although the Schwarz's approximation may fail for small samples because of its asymptotic nature, the use of SIC is generally appropriate for selecting the number of classes in image analysis. According to the SIC, merging of two regions can be considered if the decrease in the log likelihood is less than $(0.5\log n)$ multiplied by the change in the number of parameters associated with a merged class.

For the intensity process of an additive Gaussian field with diagonal covariance matrix, the cutting rule is designed on the basis of the SIC :

$$\begin{aligned}\mathrm{CR}(r,s) &= n_{r\cup s}\sum_{k=1}^{b}\ln\hat{\sigma}^2_{r\cup s,\,k} \\ &\quad -\left(n_r\sum_{k=1}^{b}\ln\hat{\sigma}^2_{r,\,k} + n_s\sum_{k=1}^{b}\ln\hat{\sigma}^2_{s,\,k}\right) \qquad (7)\\ \mathrm{CR}_{\max} &= \frac{K(1)\log n}{2}\end{aligned}$$

where $\hat{\sigma}^2_{j,\,k}$ is the kth band's sample variance of G_j and $K(1) = 2b$ when using (6) and (7).

3. Hierarchical Clustering Classification

Hierarchical clustering is an approach for step-by-step merging of small clusters into larger ones. In the classification, the image partition resulting from the local segmentor are classified into a small number of distinct states by sequentially merging two regions at each iteration. This study used a dissimilarity coefficient based on the Mahalanobis distance. The coefficient for two regions, r and s, is defined as

$$\begin{aligned}&\lambda(r,s) = M_{r\cup s} - (M_r + M_s)\\ &M_j = \sum_{k\in G_j}(\mathrm{x}_k - \bar{\mathrm{x}}_j)'\hat{\Sigma}_j^{-1}(\mathrm{x}_k - \bar{\mathrm{x}}_j) \qquad (8)\\ &\bar{\mathrm{x}}_j = \frac{\sum_{k\in G_j}\mathrm{x}_k}{n_j} \quad \text{for } j = r, s, r\cup s\\ &\hat{\Sigma}_j = \frac{\sum_{k\in G_j}(\mathrm{x}_k - \bar{\mathrm{x}}_j)(\mathrm{x}_k - \bar{\mathrm{x}}_j)'}{n_j}\end{aligned}$$

where x_k is the observation vector of the kth pixel.

No clue to the optimal number of classes is generally provided in unsupervised analyses. If the estimated number of classes is too small, regions with different characteristics will not be properly partitioned in the classified image. However, a relatively homogeneous region can be separated into a number of smaller nonmeaningful regions, if the estimated number is too large. In most studies of cluster validation, the validation criteria are based on statistical rules or model fitting approaches. However, these conventional approaches usually fail to find a parsimonious model, which is typically desirable, especially for large images with a small number of classes. A simple heuristic rule can be used an alternative for the global segmentation such that the optimal number of classes is determined at the hierarchical level where the value of the similarity coefficient changes quite markedly in consecutive iterations of the clustering procedure (Lee, 2001). An interactive approach to select the optimal number of classes in the global segmentation was introduced in Lee (2003).

4. Experiments

The proposed CN-Chain Classification (CNCC) was first evaluated using simulation data generated by the Monte Carlo method. The methodology was then applied to LANDSAT ETM+ and IKONOS data acquired from two regions on the Korean peninsula respectively.

Single/multidimensional 8-bit simulation images were generated using several different patterns by adding white Gaussian noise, whose variance is pixel-independent and region-dependent. Thus, the region-class process is characterized by the mean and variance of intensity values. The image patterns of 5 classes, which were used in this section for evaluation of the algorithm, are illustrated in Fig. 1. Fig. 1 shows 4 patterns (A, B, C, D) of 3 different sizes (1024×1024, 2048×2048, 4096×4096). The experiment used simulation images with 3 different numbers of bands (1, 3, 5). In order to represent varying noise levels in the simulation images, the signal-to-noise ratio (SNR) is defined as the ratio of the smallest intensity-level difference to the average noise standard deviation. For computational convenience, the SNR values are the same for all bands, the variances of all region-classes are identical, and the differences between contiguous levels in order of mean intensity are constant. In this experiment, the simulation images of single band were generated with 3 different SNRs of 0.5, 1.0 and 2.0, 3-band images with the SNRS of 0.3, 0.5 and 1.0, and 5-band images with the SNRs of 0.2, 0.3 and 0.5.

First, the CNCC was applied to the simulation images using 7 different levels of pyramid-structure for the multi-window operation. For 3 different numbers of bands, Fig. 2 shows the CPU times according to the pyramid level, which was obtained by averaging the computation time of CNCC for 12 images of 2048×2048, which were generated from every combination of 3 different SNRs and 4 different patterns. The best computation time was yielded for all the numbers of bands when using the level-1 structure corresponding to the base window size of 1024×1024. For 3 different sizes, the average CPU times of 12 simulation images of 3 bands are illustrated in Fig. 3. For the images of 1024×1024 and 2048×2048, the CNCC completed the algorithm with the shortest time in the level-1 structures, and the level-2 structure resulted in the best computation time for the images of 4096×4096. Both of the results show that the computation time of CNCC increases linearly by increasing the number of bands or the sizes. Fig. 4 displays the computation times of 3-band images of 2048×2048 for 3 different SNRs, which were averaged over the cases of 4 patterns, and for 4 different patterns, which were averaged over the cases of 3 SNRs. It shows that the CNCC is not affected in computational performance by the SNRs and the patterns. In the following experiments, the level-1 structure was used for the images of 1024×1024 and 2048×2048, the level-2 for them of 4096×4096.

Next, the CNCC was compared in computation time with the multistage algorithm proposed Lee (2001) (MCNC). The experiment used the MCNC with the base window size of 32×32, which had the best computational time in the pyramid structures of different levels. Table 1 illustrates the comparison of CPU time between the MCNC and CNCC for 12 3-band images of 2048×2048 generated with every combination of 3 different SNRs and 4 different patterns. It shows the computational performance of CNCC was consistently better than the MCNC's. For 3 different bands and 3 different sizes, Table 2 contains the results of the average CPU times of MCNC and CNCC for 12 images generated from every combination of 3 different SNRs and 4 different patterns.

The experiment compared the performance of MCNC and CNCC in classification accuracy for the simulation data by making the algorithms always produce the classification maps with the number of

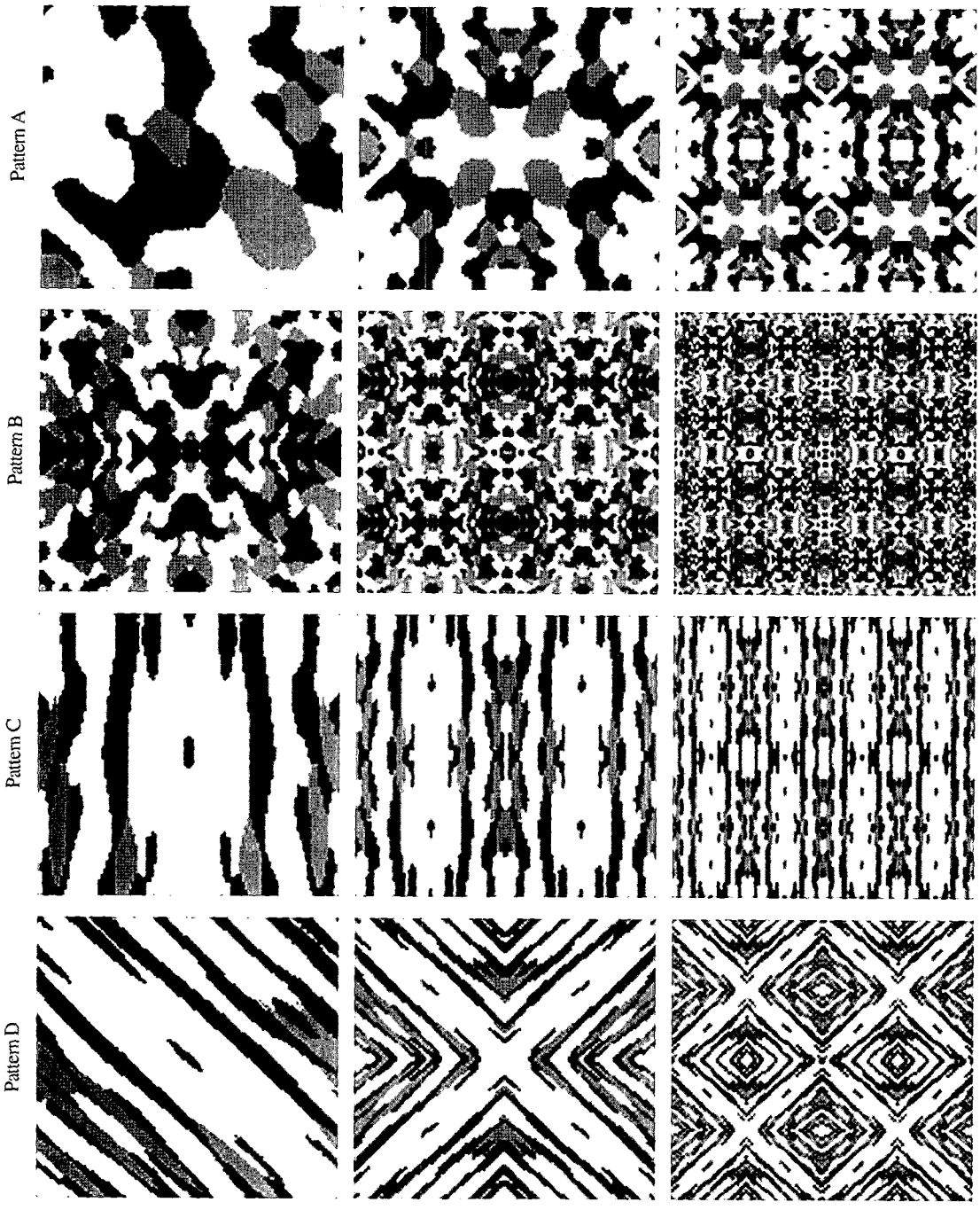

Fig. 1. Patterns for simulation data.

classes same as in the image patterns. Table 3 compares the classification errors of MCNC and CNCC for the simulation images used for the results of Table 1. For 3 different SNRS and 3 different numbers of bands, Table 4 contains the classification errors resulting from averaging the errors of 12 images generated from every

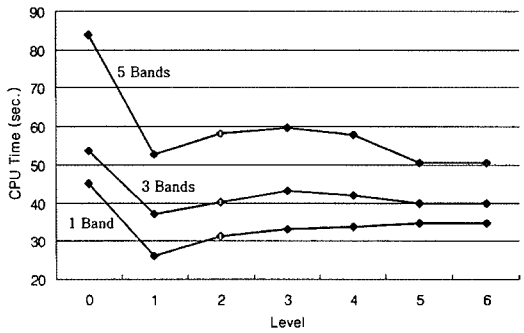

Fig. 2. Average CPU times (sec.) of CNCC according to 7 different multi-window operation levels for 12 images of 2048 × 2048 generated from combinations of 3 different SNRs and 4 different patterns.

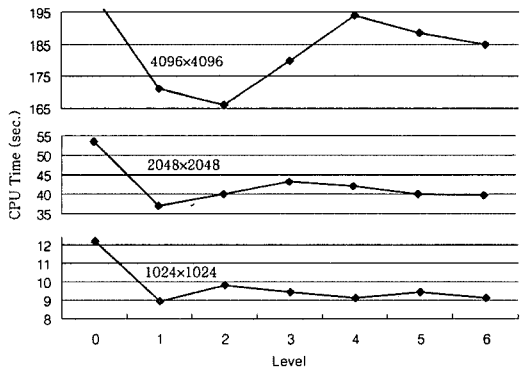

Fig. 3. Average CPU times (sec.) of CNCC according to 7 different multi-window operation levels for 12 images of 3 bands generated from combinations of 3 different SNRs and 4 different patterns.

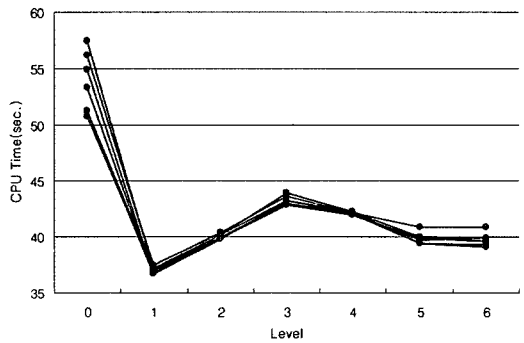

Fig. 4. Average CPU times (sec.) of CNCC according to 7 different multi-window operation levels for 3-band images of 2048 × 2048 generated from 3 different SNRs and 4 different patterns respectively.

Table 1. Comparison of CPU Time (sec.) of MCNC and CNCC for 3-Band Images of 2048 × 2048.

SNR / Pattern	0.3		0.5		1.0	
	MCNC	CNCC	MCNC	CNCC	MCNC	CNCC
A	45.73	37.48	45.89	36.86	45.53	36.78
B	43.31	37.33	43.22	36.58	43.17	36.56
C	46.33	37.64	45.95	36.94	46.08	36.81
D	45.95	37.42	46.11	36.69	45.98	36.66

Table 2. Comparison of Average CPU Times (sec.) of MCNC and CNCC for 12 Images Generated from Combinations of 3 Different SNRs and 4 Different Patterns.

Band No. / Dimension	1		3		5	
	MCNC	CNCC	MCNC	CNCC	MCNC	CNCC
1024 × 1024	8.19	6.18	10.16	8.94	12.94	12.51
2048 × 2048	37.41	26.25	45.27	36.98	56.19	52.65
4096 × 4096	184.94	141.91	203.38	166.03	244.6	228.99

Table 3. Comparison of Classification Errors(%) of MCNC and CNCC for 3-Band Images of 2048 × 2048.

SNR / Pattern	0.3		0.5		1.0	
	MCNC	CNCC	MCNC	CNCC	MCNC	CNCC
A	7.1%	6.9%	2.3%	2.5%	0.4%	0.4%
B	14.3%	14.5%	6.5%	6.2%	1.3%	1.3%
C	8.7%	7.7%	3.3%	3.5%	0.6%	0.6%
D	10.4%	11.8%	4.9%	4.6%	1.0%	1.0%

Table 4. Comparison of Average Classification Errors(%) of MCNC and CNCC for 12 Images Generated from Combinations of 3 Different Sizes and 4 Different Patterns.

SNR / Band No.	(0.5, 0.3, 0.2)		(1.0, 0.5, 0.3)		(2.0, 1.0, 0.5)	
	MCNC	CNCC	MCNC	CNCC	MCNC	CNCC
1	43.0%	42.9%	10.1%	10.4%	10.8%	10.0%
3	30.0%	30.2%	4.2%	4.2%	4.4%	4.1%
5	1.1%	1.2%	0.8%	0.8%	2.0%	1.9%

combination of 3 different sizes and 4 different patterns. In Table 4, the values in parenthesis represent the SNR associated with the number of bands. Fig. 5 displays the average error rates of CNCC of the simulation images

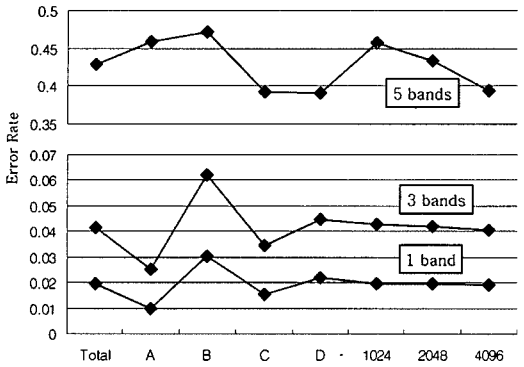

Fig. 5. Average error rates of CNCC according to 3 different numbers of bands for images of SNR = 0.5 generated from 3 different sizes and 4 different patterns respectively.

with SNR = 0.5 for 3 different numbers of bands. In this figure, the first label on X-axis (Total) represents the average rates obtained by averaging the errors in the classification results of all 12 images with SNR = 0.5 generated from every combination of 3 different sizes and 4 different patterns for each band-number. The next 4 labels of A, B, C, D represent the average rates obtained by averaging the errors in the classification for 3 images with different sizes for the corresponding patterns respectively, and the following 3 labels the average errors for 4 images with different patterns for the corresponding sizes respectively.

The agglomerative hierarchical clustering procedure requires to initially compute the coefficients of (8) for the pair candidates possible to be merged as many as $M_0(M_0 - 1)/2$ where M_0 is the initial number of segments for the global segmentor and to search the best pair with the computation time proportional to the number of all the candidates. This experiment used the maximum of 10,000 for M_0, that is, the local segmentor was forced to produce the segments less than 10,000. Fig. 6 displays the CPU times for the global segmentation according to M_0 and the second-order polynomial equation to estimate the computation time using M_0(y = Time and x = M_0 in the equation). It shows that the computation

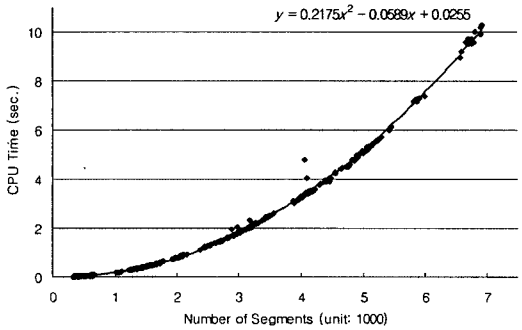

Fig. 6. CPU time vs. initial number of segments for classification.

time somewhat exponentially increased as M_0 increased. According to the estimated equation, the computation time will be more than 2,000 seconds for M_0 = 100,000.

The CNCC was applied for LANDSAT ETM+ data observed from Yongin/Nungpyung area in Kyunggi-do, Korea on September, 2000. The image data has 1587 × 1985 pixels and 9 bands including the panchromatic band. The data set of ETM+ sensor has actually 7 bands except the panchromatic band, but the data of the sixth band of Mid-IR was provided as a set of two bands. The spatial resolution of multispectral bands of 30m was modified to 15m equivalent to the resolution of panchromatic band. Fig. 7 displays the classification maps of 3 classes generated by the MCNC and CNCC respectively. The map of MCNC was produced in Lee (2001) using the data set of only 3 bands of Green, Red and NIR. The CNCC used 50.59 seconds to produce the classification map. A set of IKONOS data acquired over Kangnam area in Seoul, Korea, which has 4 mutispectral bands of 774 × 864 and a panchromatic band of 3096 × 3456, was used to produce the classification map. Fig. 8 displays the gray-scaled image of 24-bit multispectral data of Red, Green and Blue, and the 8-bit images of NIR and panchromatic band. The CNCC classified the panchromatic data of single band with the CPU time of 143.48 seconds, and the image data of 5 bands combining the mutispectral and panchromatic data with 187.20 seconds. The

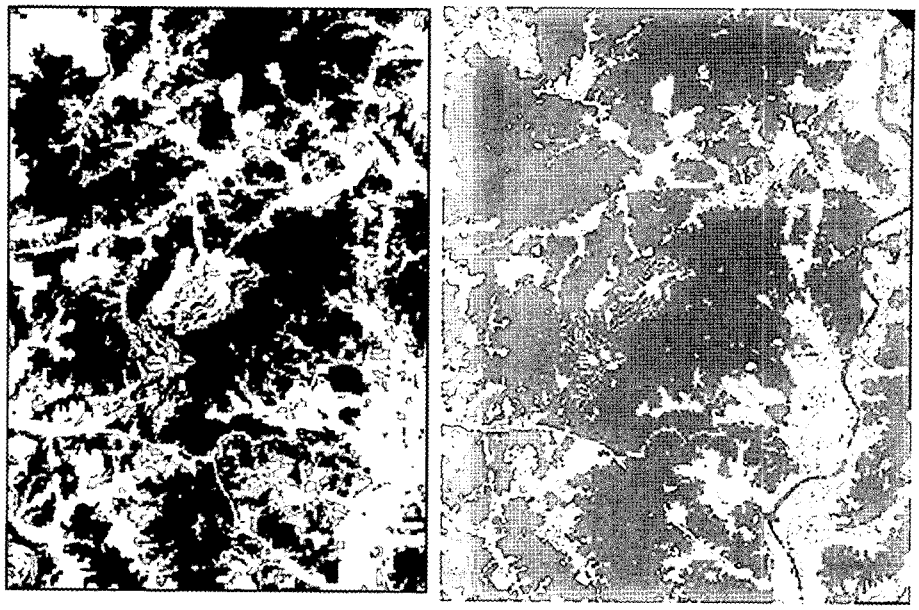

MCNC with (G + R + NIR) Bands　　CNCC with 9 Bands

Fig. 7. Classification results of 4 classes using LANDSAT ETM+ data observed from Yongin/Nungpyung area in Kyunggi-do, Korea at September, 2000.

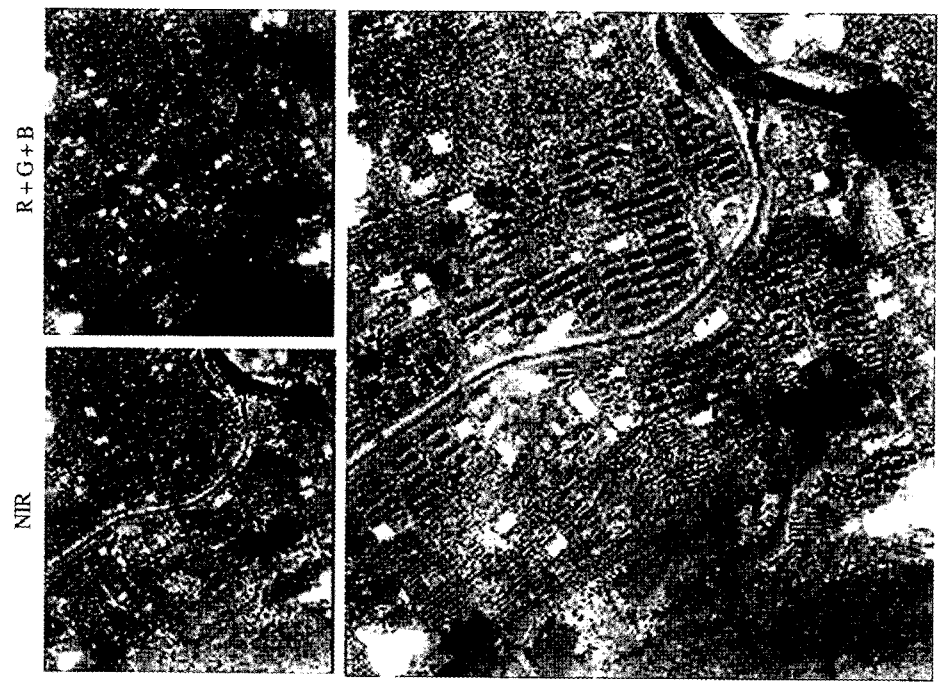

Fig. 8. IKONO images of Kangnam area in Seoul, Korea: Multispectral Image of 4m resolution (left) and panchromatric image of 1m resolution (right).

multispectral data of 4m-resolution was modified to 1m-resolution data for the 5-band data of 3096 × 3456. Fig 9 displays the classification maps of city area using very high resolution data.

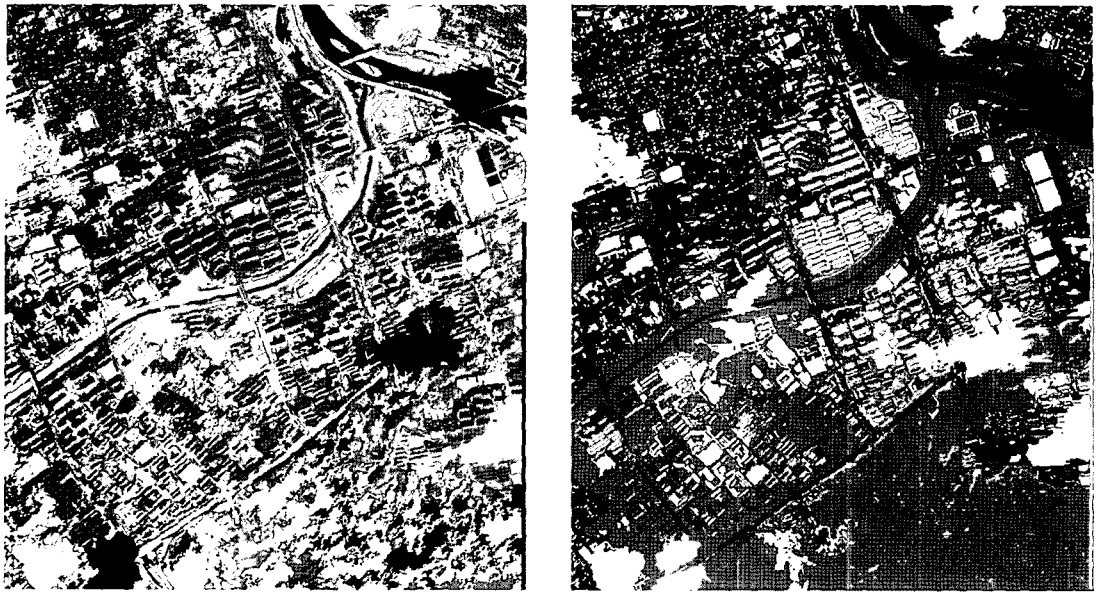

Fig. 9. Classification results with 5 classes of single band image of IKONO panchromatric data (left) and 5-band image of IKONO panchromatric+multispectral) data.

5. Conclusions

Experiments with simulation data show that the use of CN-chain improves the computational efficiency for the segmentation in the multistage algorithm, but does not affect the classification accuracy. The computational performance of both the multistage algorithms is independent on image quality or contents, but the MCNC performs differently according to the pyramid levels of multi-window operation giving the better result for the use of a higher level. Though the level of pyramid structure does not change seriously the computational performance of CNCC, it shows the worst performance with the level-0 structure and usually performs best with the level-1 structure and the level similar to the base window size of 1024×1024 for large images. As shown in Table 2, the computational improvement of the CNCC is reduced as the number of bands increased. It implies that the computational complexity of the segmentation in the multistage algorithms is much dependent on the calculation of dissimilarity measures.

The global segmentor employs the conventional agglomerative hierarchical clustering, which merges two small clusters into large one at each iteration by selecting the best pair of all possible candidates. As the initial number of segments increases, the requirement of memory for the dissimilarity coefficients and computational time for the search of the best pair exponentially increases. The initial number of segments for the global segmentor should be limited with an appropriate size by providing a maximum number of segments generated in the local segmentor.

The use of multi-channel data may be very important to improve the classification accuracy, as shown in Fig. 5. But it may be not true for the analysis of remotely-sensed data. In Fig. 7, a water stream at the very right side of image is distinguishable in the classification map of 9 bands, but the area of golf course in the center of image is more clear in the map of 3 bands. It may imply that more bands do not guarantee better results for the analysis of real remotely-sensed imagery. This fact is

also shown in the results of the application for a set of IKONOS data. The map of panchromatic band shows in detail a spatial structure of the city, while the vegetation area appears distinct in the map using the multispectral bands. It indicates that the selection of suitable feature vectors is important for real applications.

Ackknowledgements

This study was supported in part by Kyungwon University and the Korean Ministry of Science and Technology. I am appreciative to ETRI and the remote sensing laboratory of Kookmin University for providing the remotely-sensed images used in this study.

References

Adams, R. and L. Bischof, 1994. Seeded region growing, *IEEE Trans. Pattern Anal. Machine Intell.*, 16: 641-647.

Anderberg, M. R, 1973. *Cluster Analysis for Application*, Academic Press, NY.

Chang, Y-L. and X. Li, 1994, Adaptive image region growing, *IEEE Trans. Image Processing*, 3: 868-872.

Fan, J., D. K. Y. Yau, A. K. Elmagarmid, and W. G. Aref, 2001. Automatic image segmentation by integrating color-edge extraction and seeded region growing, *IEEE Trans. Image Processing*, 10: 1454-1466.

Haris, K., S. N. Efstratiadis, N. Maglaveras, and A. K. Katsaggelos, 1998. Hybrid image segmentation using watershed and fast region merging, *IEEE Trans. Image Processing*, 7: 1684-1699.

Hojjatoleslami, S. A. and J. Kittler, 1998. Region growing: a new approach, *IEEE Trans. Image Processing*, 7: 1079-1084.

Lee, S-H., 2001. Unsupervised image classification using spatial region growing segmentation and hierarchical clustering, 17:57-70 (in Korean).

Lee, S-H., 2003. Analysis of land-cover type using multistage hierarchical clustering image classification, 19: 135-148 (in Korean).

Lee, S-H. and M. M. Crawford, 2005(in press). Unsupervised Multistage Image Classification Using Hierarchical Clustering with a Bayesian Similarity Measure, *IEEE Trans. image processing*, accepted (April, 2004).

Pavlidis, T. and Y-T. Liow, 1990. Integrating region growing and edge detection, *IEEE Trans. Pattern Anal. Machine Intell.*, 12: 225-233.

Schwarz, G., 1978. Estimation of the Dimension of a Model, *Annal., Math., Statist.*, 6: 461-464.

Won, C. S. and H. Derin, 1992. Unsupervised segmentation of noisy and textured images using Markov random fields, *Comp. Vision, Graphics, Image Processing*, 54: 308-328.

Zhu S. C. and A. Yuille, 1996. Region growing, and Bayes/MDL for multiband image segmentation, *IEEE Trans. Pattern Anal. Machine Intell.*, 18: 884-900.